Synthesis of Discontinuously Reinforced Metal-matrix Composites Using Spray Atomisation and Co-injection

Enrique J. Lavernia
Department of Mechanical and Aerospace Engineering
University of California, Irvine, CA 92717

ABSTRACT

A variety of processing techniques have evolved over the last two decades to optimize the structure and properties of particulate reinforced metal-matrix composites (MMCs). Among these, spray processes offer a unique opportunity to combine the benefits associated with fine particulate technology with *in situ* processing, and in some cases, near-net shape manufacturing. Spray processing generally involves mixing reinforcements and matrix under highly non-equilibrium conditions, and as a result, these processes offer the opportunity to modify the properties of existing alloy systems, and develop novel alloy compositions. In principle, such an approach will inherently avoid the extreme thermal excursions, with concomitant macrosegregation, normally associated with casting processes. Furthermore, this approach also eliminates the need to handle fine reactive particulates, normally associated with powder metallurgical processes. The present paper discusses recent developments in the area of spray atomisation and deposition processing of discontinuously reinforced MMCs, with particular emphasis on the synergism between microstructure, mechanical properties and processing.

NOMENCLATURE

A	surface area of droplet in contact with a single particulate, m^2
A_d	droplet surface area, m^2
A_f	area fraction of *SiC* particulates, m^2
A_s	*SiC* surface area, m^2
C_p	specific heat of melt, J/kgK
C_{SiC}	specific heat of *SiC* particulates, J/kgK
d_{16}	droplet diameter equal to the upperbound of 16 pct of the droplets, m
d_{50}	mass mean droplet diameter, m
d_{84}	droplet diameter equal to the upperbound of 84 pct of the droplets, m
$f(d_i)$	mass fraction of droplets of diameter d_i
f_l	fraction liquid
f_s	fraction solid
h	heat transfer coefficient between droplets and gas, W/m^2K
$H(d_i)$	heat content of a single droplet, kJ
H_f	latent heat of fusion, kJ/kg
$H_{droplet/kg}$	total thermal per unit mass of a single droplet, kJ
H_{spray}	total enthalpy of the atomised spray at any specific location, kJ
$H_{spray,SiC}$	enthalpy of the spray in the presence of *SiC* particulates, kJ
K_a	thermal conductivity of the atomosing gas, W/mK
K_m	kinetic growth coefficient, m/sK
K_{SiC}	thermal conductivity of the *SiC* particulates, W/mK
L_a	length of interface between droplet and particulate as measured perpendicular to the droplet surface, m
L_{SiC}	characteristic length of *SiC* particulate, m
$m(d_i)$	mass of a singl droplet, kg

Received 21 May 1993

$m_{deposit}$	mass of deposit, kg
$m_{droplet,i}$	mass of droplet of diameter d_i, kg
$m_{droplets}$	total mass of droplets, kg
m_{metal}	mass of metal, kg
m_{SiC}	average mass of *SiC* particulate, kg
$n(d_i)$	number of droplets of diameter d_i
n_s	number of *SiC* particulates in intimate contact with matrix droplet
n_{SiC}	number of *SiC* particulates
N	total number of droplets
q_r	overall rate of conductive heat transfer. kJ/s
$Q_{(di)SiC,\,flight)}$	total amount of thermal energy lost by atomised droplets to the *SiC* particulates, kJ
s	distance travelled, m
$t(d_i)$	time taken by a droplet of diameter d_i from injection point to deposition point, s
T_1	temperature of the surroundings, K
T_2	temperature of the droplet, K
T	temperature, K
$u(d_i)$	velocity of droplet at the *SiC* injection point, m/s
U	overall heat transfer coefficient between *Al* and *SiC* particulate, J/m^{2}sK
C/A	apect ratio of particulates
d_o	nozzle diameter, m
Fe	particulate injection
h	heat transfer coefficient, J/m^{2}sK
J_{Fe}	mass flow rate of particulates, kg/s
J_g	gas flow rate, kg/s
J_m	metal flow rate, kg/s
K	thermal conductivity, J/msK
Q_c	heat of conduction, J
Q_h	heat of convection, J
Q_R	heat of radiation, J
T	temperature of particulates, K
V_{Fe}	exit velocity of particulates, m/s
V_g	exit velocity of gas, m/s
Z	flight distance, m
Z_i	injection distance, m
σ	Boltzmann's radiation constant, J/m^{2}sK
ε	emissivity of the surface
ρ_m	density of melt, kg/m^3
ϕ	injection angle
Δ_T	temperature gradient, k
σ_m	surface tension of melt, kg/s^2
μ_g	viscosity of gas, kg/ms
μ_m	viscosity of melt, kg/ms

1. INTRODUCTION

Research in materials science and engineering has progressively shifted towards the study and application of non-equilibrium processes in order to develop novel materials with exceptional combinations of structure and properties[1-5]. The departure from thermodynamic equilibrium typically associated with these types of processes offers a unique opportunity to the material scientist to develop otherwise unattainable combinations of structure and properties. One notable example of non-equilibrium processing is provided by spray atomisation and deposition which over the past decade has attracted considerable attention as a viable processing alternative for structural materials[6-13]. Survey of the available literature reveals that spray atomisation and deposition has been applied to numerous alloy systems, including *Mg* alloys[14-15], *Al* alloys[12,16-22], *Fe-C* alloys[23-29], *Cu* alloys[30,31], *Ni* alloys[32-36], intermetallic compounds[37-41], and more recently, particulate reinforced MMCs[42-49]. In particular, spray deposition processing of discontinuously reinforced metal and intermetallic matrix composites (IMCs and MMCs) is of interest for several reasons. Firstly, because of highly efficient heat convection during atomisation, relatively low processing temperatures can be maintained, and hence, deleterious interfacial reactions can be minimised. This provides the opportunity to process metal/ceramic combinations that would otherwise react extensively when exposed to elevated temperatures. Secondly, spray atomised and deposited materials have been reported to exhibit some of the characteristics associated with rapid solidification, namely, fine grained microstructures, increased solid solubilities, non-equilibrium phases and the absence of macrosegregation. Thirdly, spray atomisation and co-deposition processes have the potential of being utilised for near-net shape manufacturing of difficult to form materials, such as the intermetallics (for example, Ni_3Al). Spray atomisation and co-deposition processing involves mixing reinforcements and matrix in a regime of the phase diagram where the matrix contains both solid and liquid phases. In principle, such an approach

will inherently avoid the extreme thermal excursions, with concomitant degradation in interfacial properties and extensive macrosegregation, normally associated with casting processes. Furthermore, this approach also eliminates the need to handle fine reactive particulates, as is necessary with powder metallurgical processes.

During spray atomisation and co-deposition, a matrix material is disintegrated into a dispersion of droplets with an average size denoted as d_{50} using high velocity inert gas jets. Simultaneously, ceramic particulates are co-injected into the atomised spray at a previously determined spatial location (Z_i) and angle, ϕ, as shown in Fig. 1. Figure 1 also shows the primary physical properties and synthesis parameters governing the resultant average droplet size during atomisation (d_{50}); the physical characteristics and synthesis parameters of the reinforcing phase (Fe_Q); and the two principal modes of heat extraction: convection (Q_n) and conduction (Q_c). A discussion of the effects of injection conditions on the resultant distribution of reinforcing phase in the matrix will be given in the following sections. The injection distance, Z_i, is determined on the basis of numerical analysis of the fraction solid contained in the atomised matrix as a function of flight distance. This synthesis approach attempts to achieve interfacial control by injecting the reinforcing particulates at a spatial location where the atomised matrix spray contains a limited amount of volume

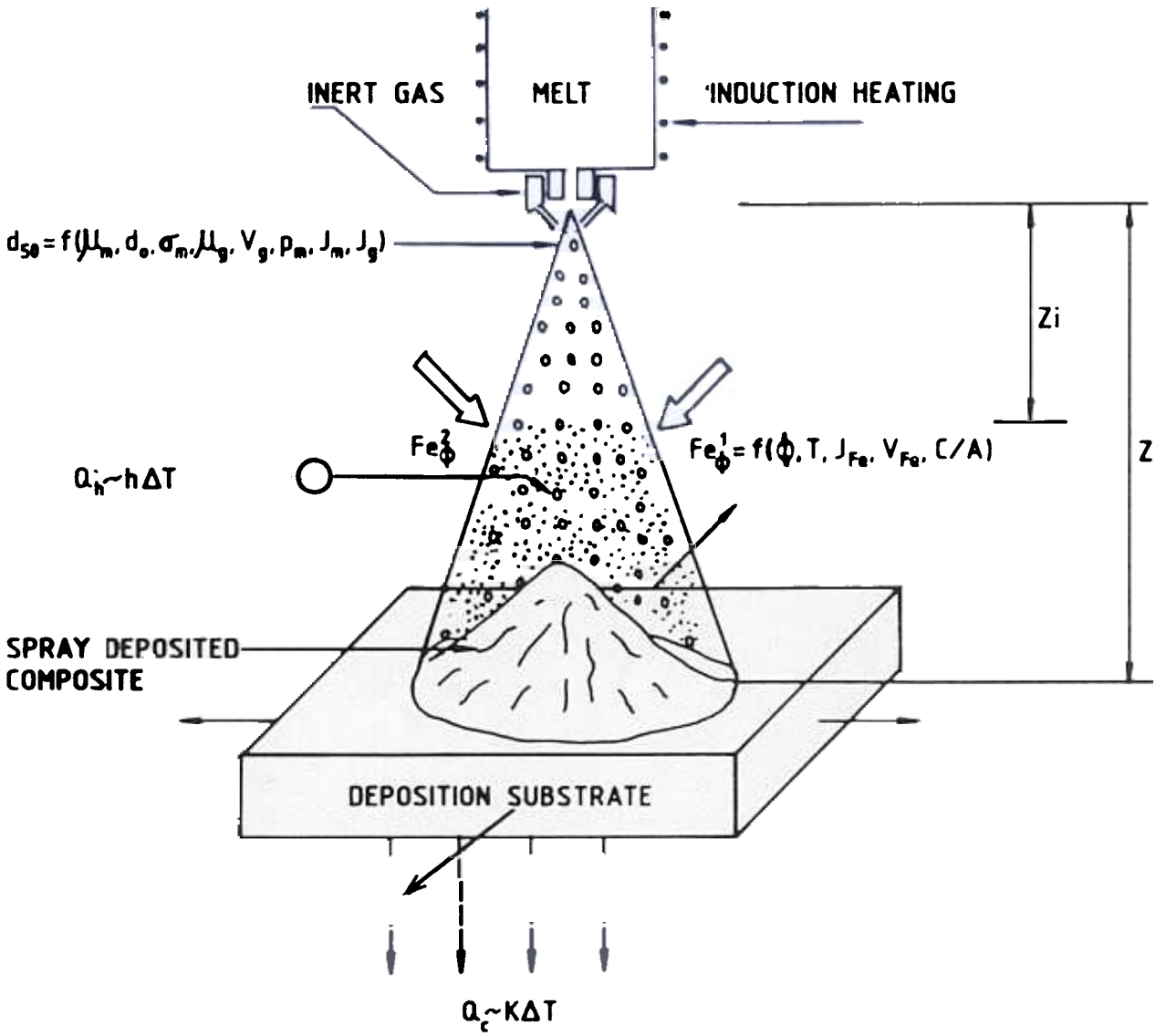

Figure 1. Spray atomisation and co-deposition processing.

fraction liquid. In this manner, contact time, thermal exposure of the reinforcing particulates to the partially solidified matrix, and interfacial reactions can be minimised. In order to avoid extensive oxidation of the matrix during processing, the experiments are conducted inside an environmental chamber.

2. SOLIDIFICATION AND MICROSTRUCTURE

The grain morphology of materials processed by spray atomisation and deposition has been generally reported to consist of equiaxed cells[6-10,14-49]. Although the formation of equiaxed grains during spray atomisation and deposition is not a well-understood phenomenon, there are two basic mechanisms that have been proposed to account for the formation of this grain morphology: (i) equiaxed grain formation in a semi-liquid/semi-solid layer on the deposition surface by dendrite arm fragmentation[7,24,27] and (ii) equiaxed grain development by growth and coalescence of dendrite fragments during solid-state cooling[39].

In the first mechanism, i.e., dendrite arm fragmentation, dendrite arm fragments are considered to be the major cause of the formation of equiaxed grains. In correlating the observed equiaxed microstructure with the dynamic processes in spray deposition, Lavernia *et al*[7,14] and Annavarapu *et al*[24,27] suggested that as a result of the incidence of solid, liquid and semi-liquid droplets, a semi-liquid/semi-solid layer develops on the deposition surface. The impact of solid and semi-solid droplets on the depostion surface provides dendrite arm fragments which may act as nucleation centres for equiaxed grains. Furthermore, Lavernia[7] proposed that the formation of equiaxed grains during spray deposition is a result of three simultaneous processes: (i) dendrite arm fragmentation, (ii) nucleation and grain multiplication, and (iii) constrained growth. First, the solid and semi-solid droplets that incident the deposition surface will deform, leading to dendrite arm fragmentation which provides nucleation centres for equiaxed grains. Second, grain multiplication occurs as a result of mechanical fracture of dendrite arms in the semi-liquid/semi-solid layer due to repeated impact of droplets, or as a result of dendrite arm remelting due to the strong turbulence developed in the semi-liquid/semi-solid layer. Third, the presence of porosity and prior droplet boundaries may restrain the migration of solid/liquid interfaces leading to constrained grain growth.

Regarding the formation of equiaxed grains during solid cooling, Liang *et al*[39] proposed that the equiaxed grains evolve from two distinct processes during solid-state cooling: (i) the homogenisation of dendrite arms that did not deform extensively during deposition, and (ii) the growth and coalescence of deformed and fractured dendrite arms. Support to this suggestion was provided by experimental and numerical results obtained with spray deposited Ni_3Al which suggest that the microstructure in the bulk spray deposited Ni_3Al is exposed to a high temperature thermal exposure during deposition. On the basis of a dendrite coarsening mechanism, the relative thermal exposure time under a particular cooling rate was calculated and converted into an equiaxed grain size from an equation of the form $d_{equ} = 15.2T^{-0.35}$; the experimental results were noted to concur with this relationship. Moreover, kinetic analyses of the experimental data obtained in this study showed that the activation energy necessary for grain growth to occur was higher than the activation energy for recrystallisation but lower than that required for diffusion. The large amount of grain boundry area associated with the dendrite morphology present in the as-solidified powders was thought to provide the necessary driving force for growth to occur in the microstructure.

Progress has been made regarding the understanding of resulting distribution of reinforcing phases during spray deposition of composite materials. In a recent study, Gupta *et al*[43] incorporated up to 20 vol per cent of SiC particulates (SiC_p) into an aluminium lithium matrix using spray atomisation and deposition. In these experiments, injection of the reinforcing phase was accomplished by entraining SiC_p in an inert gas stream using a suitably designed fluidised bed. Table 1 gives the results of image analysis of the microstructure of five distinct experiments[43].

The resultant distribution of reinforcing phases during processing of MMCs is of interest, since the mechanical behaviour of these materials will depend on the size, distribution and orientation of these phases in the matrix. In turn, it is the interaction of these reinforcing phases—typically ceramics—with the solid/liquid interface during solidification that governs the resultant distribution. In an attempt to develop an understanding of these phenomena, various investigators have studied the interaction between a moving solidification front and a ceramic

paritculate[50-56]. It follows from these studies that the rejection or engulfment of a reinforcing particulate by a moving solidification front can be predicted on the basis of four criteria: (i) thermodynamic, (ii) critical velocity, (iii) thermal conductivity, and (iv) thermal diffusivity. The results of Gupta *et al*[43], however, show that although none of the four criteria predict particulate engulfment during spray atomisation and deposition, the results of image analysis and optical microscopy studies indicate otherwise. For example, the results shown in Table 1 indicate that the interparticle spacing for the *SiC* particulates was in the 7–21.2 μm range, whereas the grain size was in the 66–72 μm range, for all the five experiments. The results of this study, which were supported by optical and scanning electron microscopy suggest that *SiC* particulates can be found both intra-and intergranularly [43]. The presence of *SiC* particulates in the centre region of the grains suggests particulate engulfment during solidification, since particulate rejection by the solidification front would result in pushing of the particulates towards the inter-dendritic regions. As a result of this discrepancy, a mechanism, termed mechanical entrapment, was proposed to explain the observed distribution of particulates in the matrix.

Gupta *et al*[43] suggested the mechanical entrapment mechanism on the basis of a comparision of the magnitude of the repulsive forces acting on a particulate as a result of the solidification front, F_r, to that of the impact forces exerted by the droplets, F_{impact} . Thus, if $F_{impact}/F_r>1$ the particulate will be engulfed; otherwise it will be rejected. The repulsive force experienced by a particulate as a result of a solid/liquid front was computed[51] as

$$F_r = -\pi r \Delta\sigma_o/(n-1) \quad (1)$$

where r is the radius of the particulate, $\Delta\sigma_o$ represents the difference in surface tension[51] and n is a constant. The impact force due to impinging droplets of size d_i was calculated from

$$F_{impact} = V(d_i)\,\rho(d_i)\,a(d_i) \quad (2)$$

where $V(d_i)$, $\rho(d_i)$ and $a(d_i)$ represent the volume, density and acceleration of a droplet of size d_i respectively. The value of the repulsive forces computed according to Eqn (1) and the impact forces computed according to Eqn (2) are shown in Table 2. In this table, d_{50} is defined as the mass mean droplet diameter of the *Al* matrix (i.e., the opening of a screening mesh which lets through 50 per cent of the mass of the powder resulting from an atomisation experiment). It can be

Table 1 Results of image analysis *Al-Li-SiC$_p$* composite[43]

Sample No.[a]	Equivalent diameter (μm)[b]				Volume fraction (%)				Interparticle spacing
	Min.	Max.	Mean	σ	Min.	Max.	Mean	σ	(λ, μm)
1A	0.57	09.00	2.70	2.01	1.92	08.33	3.49	1.82	14.48
1B	0.57	10.00	2.71	2.10	2.89	06.15	4.56	1.13	12.69
1C	0.57	12.00	2.10	1.76	4.40	13.44	7.89	1.91	07.48
2A		—Not determined—			–	–	9.60	–	08.71[d]
2C		—Not determined—			–	–	11.65[c]	–	07.91[d]
3A	0.57	11.00	2.76	2.13	4.69	7.19	6.12	0.85	11.14
3B	0.57	10.00	2.86	2.12	4.38	6.10	5.13	0.50	12.62
3C	0.57	09.00	3.34	2.16	1.34	3.16	2.49	0.54	21.16
4A	0.25	13.56	1.65	2.92	18.39	24.72	20.75	2.25	18.14
4B	0.25	09.33	1.54	2.34	3.17	07.36	05.41	1.56	25.71
5A	0.25	10.68	1.61	2.79	2.60	07.63	03.70	1.54	19.99
5B	0.25	16.95	2.27	4.24	2.77	08.95	06.00	2.29	11.89
5C	0.25	18.92	2.58	4.83	0.76	15.00	05.29	5.23	10.78

a: A, B, C designations refer to top, centre and bottom regions, respectively, of the spray deposited *Al-Li-SiC$_p$*; b: the equivalent diameter is a measure of the size of the *SiC$_p$*; c: these values of the volume fraction were determined using quantitative metallography; and d: these values were computed for a *SiC$_p$* size of 2.7 μm.

Table 2. Computed repulsive and impact forces during deposition[43]

Repulsive force (N)	Impact force* (N)	Prediction
$F_r(1\,\mu m) = 4.33 \times 10^{-6}$	$F(d_{16}) = 2.51 \times 10^{-6}$	Engulfment not possible for 1, 3 or 5 μm particulate size.
$F_r(3\,\mu m) = 1.30 \times 10^{-5}$	$F(d_{50}) = 3.00 \times 10^{-5}$	Engulfment possible for 1, 3 and 5 μm particulate size.
$F_r(5\,\mu m) = 2.16 \times 10^{-5}$	$F(d_{84}) = 3.14 \times 10^{-4}$	Engulfment possible for 1, 3 and 5 μm particulate size.

* d_{16} (30.4 μm), d_{50} (86.0 μm) and d_{84} (243.2 μm) characterise the droplet size distribution

seen from the results shown in Table 2, that the impact forces resulting from d_{16} droplets are not sufficient to overcome the repulsive forces for a large proportion of the *SiC* particulate sizes used in this study. However, the impact force exerted by d_{50} and d_{84} droplets can lead to engulfment of 1, 3 and 5μm particulates. Since the d_{50} and d_{84} droplets comprise a large proportion of the entire distribution, it can be concluded that a large proportion of the *SiC* particulates should be engulfed. These predictions were found to be consistent with the experimental findings[43].

2.1 Grain Size Effects

The co-injection of ceramic particulates during spray atomisation and deposition generally results in a marked reduction in the grain size of the composite material, relative to that of the monolithic alloy. This observation is supported by the findings of various investigators, which are summarised in Table 3. The data shown in Table 3 indicate a wide variation in results, possibly due to differences in processing parameters and alloy compositions. For example, whereas the work of White *et al* [42] and Kojima *et al* [57] suggested decreases in grain size of up to 38 per cent for *Al–2.3Li–1.2Cu–0.6Mg–0.13Zr*, in weight per cent (8090) spray atomised and co-deposited with SiC_p and B_4C particulates, Gupta *et al* [43] reported a 67 per cent decrease in the grain size of as-spray atomised and deposited *Al–Li–*SiC_p material, relative to that observed for the unreinforced *Al–Li* matrix. The relatively small difference in grain size between the reinforced and unreinforced materials reported by Ibrahim *et al* [58] was attributed to the higher gas atomisation pressure and smaller metal delivery tube diameter used during the processing of the monolithic material (1.36 MPa and 3.04 mm) relative to that used for the MMC material (1.2 MPa and 3.30 mm). It is evident that an increase in gas atomisation pressure coupled with a decrease in the diameter of the metal delivery tube, will effectively decrease the droplet size formed during atomisation. The higher quench rate associated with smaller droplet diameters will promote extensive presolidifications

Table 3. Results of grain size measurements as reported by various investigators

Matrix composition reference (wt. %)	Reinforcement	As spray deposited grain size			
		Monolithic (μm)	MMC (μm)	% Change	Ref. No.
Al-2.1 *Li*	SiC_p (3 μm)[a]	207	67	68	43
6061 *Al*	SiC_p (3 μm)	22-25	22		58
8090 *Al*	SiC_p & B_4C	48	30	38[b]	42, 57
Al-4*Li*-1*Mg*	SiC_p (3 μm)	22	15	32	59

a : average *SiC* particulate size, b : measure from micrographs

prior to impact with the deposition surface, with concomitant refinement in the spray deposited microstructure.

In view of the complex thermal, fluid, and solidification phenomena involved during spray atomisation and co-deposition it is highly improbable that the observed reduction in grain size can be attributed to a single mechanism. Most likely, the observed changes in microstructure can be attributed to the combined effects of several, non-linear mechanisms. One approach that may be utilised to provide insight into the effects of the ceramic particulates on the microstructural evolution during spray deposition, is to decouple the thermal, momentum and solidification phenomena into three distinct mechanisms: solidification effects, thermal effects, and solid-state cooling effects which are discussed in more detail in the following paragraphs.

Regarding the effects associated with the energetic co-injection of the ceramic particulates on the solidification behaviour, our understanding is, at best, speculative. For example, it is anticipated that the transfer of kinetic energy during impact of an undercooled droplet with an SiC_p will catalyse heterogeneous nucleation of the solid phase. In related studies[60], it has been proposed that there is a population of catalysts, which result from surface oxidation processes during atomisation, that decrease the possibility of achieving the large undercoolings required for homogeneous nucleation. Therefore, it is likely that the presence of a distribution of SiC_p and the ensuing effect on solidfication processes, will increase the volume fraction solidified during impact. This suggestion is actively being pursued by determining the thermal gradients that are induced in an atomised droplet as a result of the presence of one or several ceramic particulates.

3. MECHANICAL BEHAVIOUR

The mechanical response of spray deposited metals and composites is actively being investigated by a number of researchers around the world. Inspection of the available scientific literature immediately reveals active or nascent research programs in France, Germany, India, Italy, Japan, Korea, North and South America, the United Kingdom, and Switzerland, to cite a few notable examples. In the following sections, a succinct review of results obtained for room and elevated temperature alloys is presented.

3.1 Room Temperature Mechanical Behaviour

Regarding the room temperature mechanical behaviour of spray atomised and deposited MMCs, some preliminary results are available[42,57-59]. Ibrahim *et al* [58], for example, studied the microstructure and mechanical properties of spray atomised and deposited 6061 Al/SiC_p materials, reinforced with 3 and 15μm particulates. One example of the typical microstructures observed in this study is shown in Fig. 2. Although not evident from Fig. 2, the grain morphology of the as-spray atomised and deposited material was equiaxed and the average grain size was reported to be 22 μm.

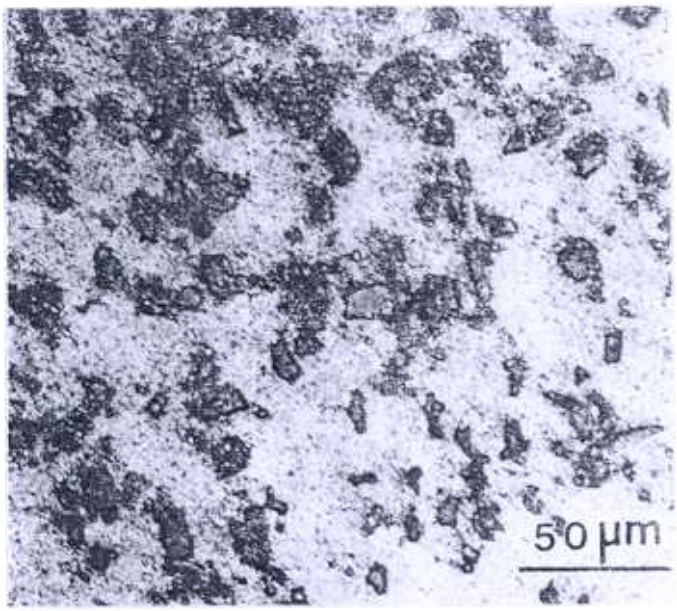

Figure 2. Optical micrograph showing microstructure of spray automized and deposited 6061 Al-SiC_p material.

The results of Ibrahim *et al* [58] also show that the presence of SiC_p alters the ageing response of the spray atomised and deposited materials, relative to that observed for unreinforced alloys. The results of this study, which are consistent with those reported by other investigators [61-63], suggest that the ageing time required to attain maximum hardness was significantly reduced in the reinforce materials, when compared to that of the unreinforced alloys. This behaviour has also been noted in MMCs processed by powder metallurgical

means[61] and has been attributed to the presence of a well defined dislocation substructure[61,63]. Numerous studies have shown[63,64] that although the dislocation density found in as-quenched, age-pardonable *Al* alloys is low, typically less than 10^5/cm, the dislocation density in reinforced *Al* matrices is[65] of the order of 10^{13}/cm. Following spray atomisation and deposition, Ibrahim *et al*[57] studied the room temperature behaviour of the hot extruded materials and noted an increase in tensile strength and decrease in tensile elongation with area fraction of SiC_p. This finding is consistent with the increase in dislocation density, with concomitant increase in dislocation particle interactions, accompanying an increase in volume fraction of reinforcements.

In related work, White *et al*[42], studied the structure and properties of a spray cast *Al-Li-Cu-Mg-Zr* alloy (8090 designation) reinforced with *SiC* and B_4C particulates. The mechanical properties of the spray cast and hot extruded materials are summarised in Table 4, and compared to those of equivalent ingot alloys. The results show that the most significant property improvements was in the value of the elastic modulus, where the value of the spray cast material was approximately 25 per cent higher than that of the corresponding ingot alloy. Further improvements in the mechanical behaviour of the spray cast materials were also achieved by introducing cold deformation prior to ageing[42].

3.2 Elevated Temperature Behaviour

Dispersion strengthened elevated temperature *Al* alloys derive their strength and thermal stability from the presence of a dispersion of nanometer-size particles that effectively impede dislocation motion during deformation. The strengthening characteristics of these particulates at high temperature are dependent on their ability to resist coarsening, and therefore low diffusivities and limited or no equilibrium solid solubility are desirable[66]. The relatively high quench rates present during spray atomisation and deposition processing have allowed investigators to utilise this synthesis approach to process high temperature *Al* alloys containing a fine dispersion of relatively insoluble phases[67,68]

Among the family of transition metal high temperature alloys, *Al-Ti* alloys are acitvely being studied as a result of their attractive combination of elevated temperature properties[69-71]. These materials derive their excellent strength, ductility, and creep resistance from their fine grain structure and dispersion of Al_3Ti particles, in combination with the low solid solubility (0.8 at per cent) and low diffusivity (3.86×10^{-5} at per cent cm^2/s) of *Ti* in *Al*[72]. In order to curtail the formation of coarse primary Al_3Ti, rapid solidification must be employed to extend the solid-state solubility of titanium in aluminium. Gupta *et al*[68], for example, noted that the amount of *Ti* in solid solution in *Al* could be increased over those achievable by equilibrium solidification, by using spray atomisation and co-deposition. A summary of the elevated temperature mechanical behaviour of the spray atomised, deposited and hot extruded *Al-Ti* alloys (SD) reported in this study is shown in Table 5, and compared to those of equivalent materials prepared by powder metallurgy (PM) and mechanical alloying (MA). The results shown in Table 5 for the *Al-4Ti* and *Al-2.3Ti-SiC*$_p$ materials were obtained after a 99 hr anneal, followed by mechanical testing at the designated temperature. The results in Table 5 show that the elevated temperature properties of the spray deposited materials compare favourably to those of the PM

Table 4. Room temperature mechanical properties of spray atomized and extruted 8090

Material	Volume fraction	σ_{UTS} (MPa)	σ_{YS} (MPa)	Elongation (%)	E (MPa)
8090		520	480	5.0	79.5
8090	12[a]	529	486	2.6	100.1
8090	11[b]	445	410	1.6	98.1

a : *SiC* particulate size used here was 13 μm, and b : B_4C particulate size used here was 13 μm

Table 5. Elevated temperature mechanical properties of spray atomized and extruted *Al-Ti-SiC* materials[68]

Material	Temperature (°C)	σ_{UTS} (MPa)	σ_{YS} (MPa)	Elongation (%)	Reference No.
Al-2.3*Ti*-SiC_p (Spray deposited) (V_f = 6-8%)	25	200	198	7	68
	250	130	116	11	
	350	51	48	18	
	450	24	22	32	
Al-4.0*Ti*[a] (Spray deposited)	25	250	235	7	68
	250	127	106	24	
	350	57	51	23	
	450	20	18	40	
Al-4.0*Ti* (Powder metallurgy)	25	180	145	23	71
	200	100	95	22	
	300	65	59	30	
	400	42	35	30	
Al-4.0*Ti* (Mechanical alloying)	25		320		71
	160		280		
	240		190		
	290		170		
	350		150		

a : all compositions are given in wt%

materials, are superior to those of the ingot materials, but are inferior to those of the MA materials (although the elongation behaviour of the MA materails was not reported). The higher thermal stability of the spray atomised and deposited materials, relative to that noted for the cast ingot and extruded material, was attributed to the faster quench rates, with concomitant microstructural refinement resulting from the spray deposition stage. This is supported by the sharp reduction in grain size and the absence of primary Al_3Ti phase observed for the as-spray deposited reinforced material, relative to that of the as-cast *Al-Ti* ingot.

4. HEAT TRANSFER CONSIDERATIONS

Over the past several years, various investigators[27,30,47,48,73-78] have formulated models of the various heat transfer, solidification, and momentum phenomena associated with spray atomisation and deposition processing. These models may be utilised to estimate droplet size distributions, droplet velocities, positions, temperatures, cooling rates, dendrite arm spacings (DAS), and solidification time, t_f, as a function of processing conditions. In these models, computation of the droplet size distribution is generally accomplished by utilising modifications to the original correlation proposed by Lubanska for predicting variations in powder size with processing parameters. Although most of these models either incorporate a number of limiting assumptions, such as small Biot numbers, limited undercooling, or are based on simplistic thermal energy arguments, i.e., enthalpy formulations, they provide some insight into fundamental solidification phenomena during atomisation. The ultimate objective of these models is to predict the thermal and solidification behaviour of droplets as a function of flight distance. This information may then be utilised to understand the evolution of the microstructure, and eventually to optimize the processing parameters during spray atomisation of deposition.

Mathematical modelling of substrate growth due to spray impingement has been conducted by Gutierrez *et al* [74], who have advanced to fundamental models to describe the thermal behaviour of both the preform and the individual splats. Specifically, they have discussed the Continuum Model, where the behaviour of the individual droplets is averaged, and an Individual Droplet Model that takes into account temperature gradients in the individual splats. The Continuum Model is reduced to the solution of the one-dimensional, unsteady energy equation for the enthalpy where the phase-change is taken into acount by a step change at the melting point. The boundary conditions involve a

simple convection cooling type of equation at the deposit-substrate interface, and the combination of enthalpy inflow from the spray, convection and radiation at the upper surface. The Individual Droplet Model considers a droplet that arrives at the top surface, flattens very rapidly, compared with the time between successive arrivals, and proceeds to exchange energy with the deposit to eventually solidify. The one-dimensional, unsteady energy equation is again used for each individual splat, while the initial and boundary conditions are modified accordingly.

Modelling of the thermal and hydrodynamic behaviour of droplets in flight and to predict their condition on arrival at the substrate has been conducted by a number of investigators[27,30,75-78]. They consider each droplet as if it were isolated from the others, and solve a one-dimensional trajectory equation including droplet drag and gravity. A correlation is used for the drag coefficient. The thermal interaction between the gas and the droplet is computed by means of the Ranz-Marshall correlation for the Nusselt number and the undercooling and solidification of the droplets is taken into account by letting the transfer heat to the gas until the nucleation temperature is reached. After nucleation, the droplet recalesces by absorbing the latent heat released by the solidifying metal. This process continues until the rate of heat release equals the rate of convective cooling to the gas.

Lawley *et al* [30] have presented an integral model that encompasses the various processes involved in spray casting in a modular fashion. These processes are: atomisation modelled by an empirical correlation; spray which follows the model described in the previous paragraph; droplet consolidation which addresses the sticking efficiency of the droplets onto the deposition surface by means of a sticking efficiency, and which has a geometric and a thermal component; the shape model dynamically predicts the evolution of preform shape for different combinations of substrate and spray motion; the preform solidification model, employs a 2-D, moving-boundary analysis to predict the temperature and liquid fraction profiles in the preform; the microstructure model, computes the segregate spacing in the final deposit from the local solidification time using standard DAS *vs* t_f relationships.

In related studies, Lavernia *et al* [47,48,76-78] have developed a simplified mathematical model of the spray atomisation and deposition processes that addresses both the heat flow during gas atomisation[76], and the formation of the deposit[77]. In the gas atomisation model, these authors assume instantaneous atomisation, droplet sphericity, non-interacting droplets, a cooling law governed by a film coefficient on the droplet surface, uniform temperature distribution inside the droplets, and a small degree of undercooling. For the modelling of the deposit formation, the authors utilise a finite difference method based on enthalpy formulation and the assumptions that one- dimensional heat flow in the direction of the substrate thickness, uniform and constant deposition rate, and specified temperature boundary condition at the upper substrate surface, given by the average of falling-droplet temperatures. This model predicts the effect of the important parameters on the resulting microstructure.

4.1 Preliminary Results Obtained with *Al*-1.0 weight per cent *Li/SiC*

In order to provide insight into the transfer of thermal energy during spray atomisation and co-deposition, and its subsequent effect on microstructure, Gupta *et al* [47,48]formulated a heat transfer model to quantify the changes in thermal energy of an atomised droplet distribution derived from the presence of a distribution of randomly mixed ceramic particulates. The degree of complexity associated with high spray densities necessitated the incorporation of a number of simplifying assumptions into the thermal and momentum equations. In particular, the treatment of an atomised spray as a collection of individual droplets, with no interactions among each other, is perhaps most limiting. Nevertheless, from a conservation of thermal energy standpoint, the results provide insight into the effects of ceramic phases on the evolution of microstructure during impact with a deposition surface. In this study, first the droplet temperature is calculated on the basis of an enthalpy model described elsewhere[47,48,78] and then the thermal energy content of the atomised spray can be computed as follows. The specific heat of the matrix material (aluminium alloy), C_p (kJ/kg), can be calculated from

$$C_p = 0.7661 + 0.46145 \times 10^{-3} T \quad T \leq 933.2\,K$$
$$C_p = 1.086 \quad T \geq 933.2\,K \qquad (3)$$

Then, the total thermal energy per unit mass of a single droplet, $H_{droplet/kg}$, can be obtained from

$$H_{droplet/kg} = \int_{T_1}^{T} C_p dT + f_1 \Delta H_f \quad (4)$$

From Eqn (4), the heat content of the droplet of mass, $m(d_i)$ can be computed from

$$H(d_i) = H_{droplet} = m(d_i) \left[\int_{T_1}^{T} C_p dT + f_i \Delta H_f\right] \quad (5)$$

The total enthalpy of the atomised spray at any spatial location, can be computed from information on the droplet size distribution as

$$H_{spray} = \Sigma n(d_i)\, H(d_i) \quad (6)$$

In Eqn (6) the number of droplets of diameter d_i, $n(d_i)$ can be calculated from

$$n(d_i) = \frac{m_{metal} \cdot f(d_i)}{-} \quad (7)$$

Therefore, the total number of droplets for a given distribution, N, can be calculated as

$$N = \Sigma\, n(d_i) \quad (8)$$

Similarly, the number of *SiC* particulates can be calculated from

$$n_{(SiC)} = \frac{\text{wt \% } SiC \cdot m_{deposit}}{100 \times m_{SiC}} \quad (9)$$

The number of *SiC* particulates in intimate contact with a matrix droplet, n_s, can be computed from

$$n_s = \frac{0.5 A_f A_d}{A_s} \quad (10)$$

It is worth noting that the results obtained using Eqn (10) were noted to be in excellent agreement with those determined experimentally. Once the number of *SiC* particulates in contact with one matrix droplet were determined, and assuming Newtonian conditions (i.e., the temperature gradient within the droplet in negligible), the overall rate of conductive heat transfer, $\dot{q}_r$, can be computed from

$$\dot{q}_r = U A (T_2 - T_1)$$

The value of overall heat transfer coefficient, U, used in Eqn (11) can be obtained from

$$U = 1/(L_a/K_a + L_{SiC}/K_{SiC})$$

In order to determine the magnitude of the overall heat transfer of thermal energy, one must consider in detail the effects of the *SiC* particulates on the droplets. The *SiC* particulates will have two opposite effects on the transfer of thermal energy from the matrix droplets. On the one hand, since the ceramic particulates are injected at room temperature, a portion of the thermal energy losses can be accounted for by considering conductive heat transfer from the droplet to the particulates. On the other hand, however, the presence of ceramic particulates on the surface of the atomised droplets will inhibit convective heat transfer from the droplets to the atomisation gas. Therefore, it is necessary to compensate for the rate of conductive heat transfer computed from Eqn (11). This was achieved by subtracting the value of the effective convective heat transfer due to the presence of *SiC* particulates, from the rate of conductive heat transfer. The effective convective heat transfer due to the presence of *SiC* particulates q_e can be computed from

$$\dot{q}_e = h A (T_2' - T_1)$$

In turn, one can take the value of $\dot{q}_r$ *and* $\dot{q}_e$ and multiply it by the time of flight t, as determined from

$$s = u(d_i) \cdot t + \frac{1}{2} g \cdot t(d_i)^2$$

and compute the total thermal energy transferred from the atomised droplets to the ceramic particulates, during flight. Therefore the total amount of thermal energy lost by the atomised droplets to the *SiC* particulates, $Q(d_i)$ (*SiC*, flight), is given by

$$Q(d_i)_{(SiC,\ flight)} = \dot{q}_r t(d_i) n_s - \dot{q}_e t(d_i) n_s \quad (15)$$

$$Q(d_i)_{(SiC,\ flight)} = (q_r - q_e)\, t(d_i) n_s \quad (16)$$

The total amount of thermal energy transferred during flight, Q_{Total}, can be calculated as

$$Q_{Total} = \Sigma\ Q(d_i)_{(SiC,\ flight)}\ n(d_i) \qquad (17)$$

In this study, the percentage heat dissipated during flight as a result of the presence of *SiC* particulates, $Q_{(SiC,flight)}$, was calculated from:

$$Q_{(SiC,\ flight)} = \frac{Q_{Total(SiC,\ flight)}}{H_{spray}} \times 100 \qquad (18)$$

where $Q_{Total(SiC,\ flight)}$ represents the total amount of thermal energy transferred during flight. A more extensive discussion of the mathematical details can be found elsewhere [47,48]. The results summarised in Table 6 show that co-injection of a distribution of *SiC* particulates into an *Al* spray will decrease the average enthalpy at impact by 10 per cent, relative to that for the unreinforced spray. Furthermore, the results found in this study also show that 8 per cent of the thermal energy was transferred to the *SiC* particulates after deposition. The equations used by Gupta *et al* [47,48] incorporate a number of assumptions which were necessary as a result of the high degree of complexity associated with high spray densities. In particular, the details associated with the effects of the ceramic particulates on the temperature and fraction solid of the atomised droplets during liquid cooling, nucleation and recalescence, two phase solidification, and solid state cooling, were not addressed; alternatively, the problem was postulated from a conservation of energy standpoint.

It is unlikely that the computed 20 per cent decrease in spray enthalpy alone can be utilised to explain the differences in grain size commonly reported for these materials (see section 2.1). In addition, one must also address the effects of the particulates on the resulting grain size and morphology during solid-state cooling. For example, it is probable that the presence of *SiC* particulates will decrease the rate of grain growth during solid-state cooling. This mechanism appears to be important in view of results reported elsewhere, which suggest that the presence of a dispersion of ceramic phases in an *Al-Li* matrix will decrease the rate of grain boundary during solid-state cooling, effectively promoting a fine grain size [47,48].

In related studies, Gupta *et al*[68], used x-ray diffractometry to study the effects of the reinforcements on the excess solid solubility of *Ti* in *α Al*, and showed that the spray atomised and deposited *Al*–4.0 weight per cent *Ti* material retained 0.8 weight per cent *Ti* in solid solution, whereas the as-spray atomised and deposited *Al*–1.2 weight per cent *Ti-SiC*$_p$ material retained up to 1.2 weight per cent *Ti* in solid solution. The difference in the amount of *Ti* retained in solid solution in the reinforced material, relative to that observed for the unreinforced material, was discussed in terms of the difference in heat flow conditions between the two materials[68].

It is concluded that firstly spray atomisation and deposition processing has the potential of being utilised to improve the structure and properties of existing alloy systems, either through the addition of secondary particulates, such as ceramics, or through modifications to the microstructure. Secondly, preliminary results from experimental and numerical studies suggest that the transfer of thermal energy during atomisation, and subsequently, during deposition has an important effect on the ensuing microstructure.

Table 6. Results of the heat transfer model for reinforced and unreinforced *Al-Li* material[47]

	Flight distance		
	0.21 m[(a)]		After deposition
Spray enthalpy (kJ/kg) (*Al-Li* material)	1230	1094	
Spray enthalpy (kJ/kg) (*Al-Li-SiC*$_p$ material)	1230	984	904
Percent heat transferred due to the presence of *SiC*$_p$		10 %	8 %

a : *SiC*$_p$ injection distance, and b : deposition distance

5. INTERFACIAL BEHAVIOUR IN Ni_3Al/TiB_2

Recently, Liang *et al* [79,80] studied a Ni_3Al/TiB_2 composite processed by spray atomisation and co-deposition, with particular emphasis on the interfacial reaction behaviour between the Ni_3Al matrix and TiB_2 particulates. During elevated temperature annealing, a distinct interfacial reaction zone formed between Ni_3Al and TiB_2 in both atomised Ni_3Al/TiB_2 powders and co-deposited Ni_3Al/TiB_2 materials which has been shown in Fig. 3. SEM/EDS analyses, indicated that this interfacial reaction product consisted of an Ni_3Ti phase (solid solution of intermetallic Ni_3Ti with Al substituting for Ti). Extended exposure of the IMCs to elevated temperatures resulted in the formation of an $NiTi$ phase. The thickness of the interfacial reaction zone between Ni_3Al and TiB_2 (R in Fig. 3) increased with annealing temperature and time; the parabolic

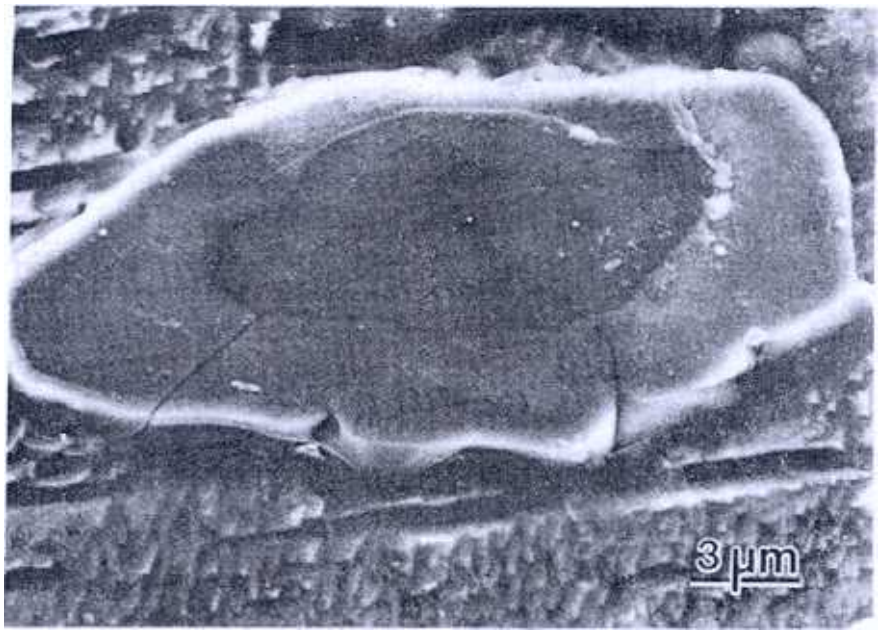

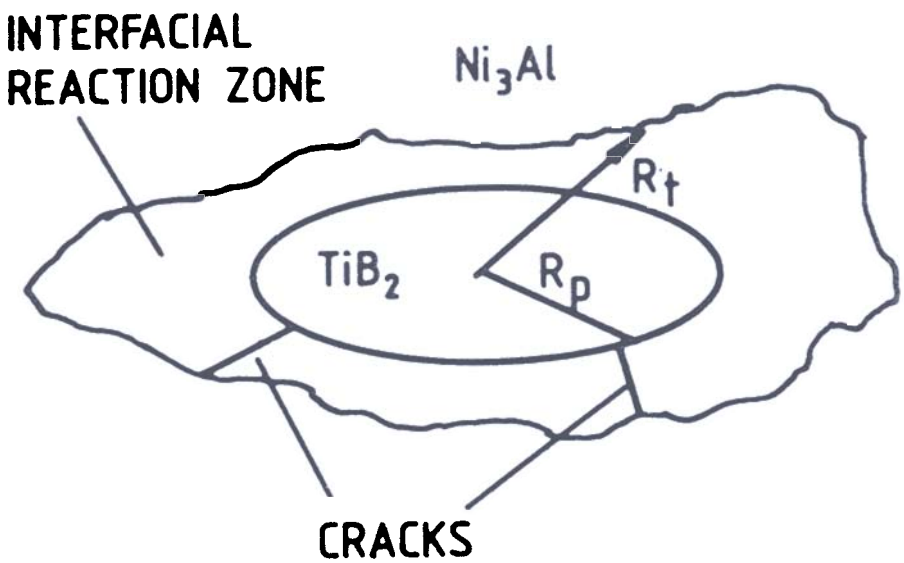

Figure 3. Interfacial reaction zone between Ni_3Al matrix and TiB_2 particulates observed in the Ni_3Al/TiB_2 composites after annealing at 1403 K for 30 minutes: (a) spray automised and co-deposited samples at a location near the substrate, and (b) schematic diagram illustrating the determination of the radius of the particulate, R_p, and the radius of the particulate and reaction zone, R_t.

relationship between the thickness of the interfacial reaction zone and annealing time suggested that diffusion through the interfacial reaction zone was the rate limiting step for the growth of this reaction zone. The diffusion of *Ni* was suggested to be the rate control step in this interfacial reaction. A low interfacial reaction activation energy, 61.5 kJ/mol, was calculated indicating fast growth of this interfacial reaction zone. The interfacial reaction kinetics between Ni_3Al and TiB_2 during annealing were noted to obey the equation: $x(t,T) = 12.8.\exp(-7400/T).t^{1/2}$.

6. INTERACTION MECHANISMS BETWEEN DROPLETS AND CERAMIC PARTICLES

In recent studies, Wu *et al* [46] addressed interactions that occur when ceramic particles are co-injected into an atomised spray consisting of solid, liquid and partially solid droplets. To that effect, *Al*-4 weight per cent Si/SiC_p composite droplets were synthesised using a spray atomisation and co-injection approach and their solidification microstructures were studied in detail both qualitatively and quantitatively. The primary results obtained in this study are summarised and discussed.

In the process of spray atomisation, droplets may experience very different thermal histories because of two reasons: (i) droplet diameter may affect both nucleation temperature and the rate of solid phase formation since it influences the rate of heat extraction, and (ii) the existence of heterogeneous nucleation catalysts, which reduce the achievable undercooling level that can be achieved by a volume of liquid. It is generally agreed that the heat extraction rate experienced by liquid droplets will remain relatively unchanged, if their diameters are similar. The extent of undercooling, however, may vary drastically from droplet to droplet. The nucleation of a solid phase in a droplet may occur by either homogeneous or heterogeneous nucleation. Under practical experimental conditions, only a small fraction of droplets may achieve the undercooling level that is theoretically required for the attainment of homogeneous nucleation. Therefore, most droplets will solidify under heterogeneous nucleation conditions. Nucleation catalysts cannot be totally eliminated from the melt, they may reduce the nucleation energy barrier resulting in nucleation at low undercoolings. For a particular droplet, the heterogeneous nucleation undercooling achieved depends on the chemistry, density and distribution of the nucleation catalysts. Such factors make it difficult to evaluate the nucleation temperatures of droplets during atomisation.

Wu *et al* [46] provided interesting insight into the overall behaviour of atomised droplets by treating the problem of undercooling as a range of temperatures. The upper limit of undercooling may be correlated to the homogeneous nucleation temperature. The average heterogeneous nucleation undercooling can be correlated to the heterogeneous nucleation temperature. Under such conditions, the upper limit of undercooling is given by $\Delta T = T_L - T_{homo}$ and the average heterogeneous nucleation undercooling can be approximated by $\Delta T = T_L - T_{hetero}$, where T_{homo} and T_{hetero} represent the homogeneous and heterogeneous nucleation temperatures, respectively. These two undercoolings indicate the temperature range where nucleation will most likely begin. Once the nucleation temperatures have been determined, the solidification conditions of the droplets may be readily predicted.

In the case of homogeneous nucleation, the level of undercooling depends on both the cooling rate as well as the diameter of droplet. It is reasonably well established that higher cooling rate generally helps to achieve a higher homogeneous nucleation undercooling. Droplet diameter affects undercooling in two ways:

(a) It defines the volume of liquid phase in which thermal fluctuations result in the formation of nuclei of critical size. The probability of forming a nucleus above the critical size increases with increasing available liquid volume. This causes a decrease in undercooling with increasing droplet diameter, and

(b) Droplet diameter also influences the cooling rate experienced by the droplets before the onset of solidification. Further more, the cooling rate defines the time period during which the liquid will remain between the liquid and the nucleation temperatures.

The estimation of the temperatures required for homogeneous nucleation undercooling can be deduced from the classical treatment of homogeneous nucleation rate by Hirsh[81], and Thompson and Spaepen[82]. The rate of homogeneous nuceation, I_{homo}, is given by

$$I_{homo} = (D_L N_v / a_0^2) \exp[-(\Delta G^*/k_B T)] \quad (19)$$

where ΔG^* is the free energy barrier for nucleation, k_B is Boltzman constant, T is temperature, D_L, N_v and a_o represent the liquid diffusivity, the number of liquid atoms per unit volume and atomic diameter, respectively. The pre-exponential part of Eqn (19), changing little from system to system, has been estimated to be of the order of $10^{41} m^{-3}s^{-1}$ by theoretical calculations[81-83]. The typical experimental value is of the order of $10^{46}/m^3s^1$. Following thermodynamic considerations, the free energy change ΔG^* due to the formation of a nucleus of critical size can be expressed in terms of undercooling as

$$\Delta G^* = \frac{16\pi\sigma_{SL}^3}{3} V_m^2 T_L^2 / (\Delta H_f^2 \Delta T^2) \qquad (20)$$

where σ_{SL} is the interfacial energy between solid and liquid phase, ΔT is undercooling, V_m and H_f are the molar volume and the molar heat of fusion, respecitvely.

In general, for given nucleation kinetics, the probability of forming a solid phase nucleus in a particular volume of liquid phase is proportional to the nucleation rate, I, volume of the liquid, V_L, and time period, t. The time, represents the period $0.01\ \Delta T/T$ during which the system is in the temperature regime between T_L and T_N where T_N is the nucleation temperature and $\dot{T}$ is the cooling rate. The total number of nuclei, n, formed during this time period is given[83] by

$$n = \frac{1}{\dot{T}} \int_{T_N}^{T_L} I(T)\, dT \qquad (21)$$

The criterion for nucleation undercooling can be established by setting $n = 1$ in Eqn (21), i.e., nucleation starts when the first nucleus appears from the undercooled liquid. By simplification, $I(T)$ can be expanded[81] around the nucleation temperature, T_N. Using the first order approximation of Eqn (21)

$$\frac{0.01 I V_L \Delta T}{T} = 1 \qquad (22)$$

If Eqn (22) is applied to spray atomisation, the liquid phase takes the form of spherical droplets. The liquid volume in this case is defined by the droplet diameter. Combining Eqns (20), (21) and (22) produces the following relationship between undercooling, cooling rate and droplet diameter

$$\Delta T_r^2 = \frac{16\pi\sigma_{SL}^3 V_m^2}{3k_B T_N \Delta H_f^2 \ln[5\times10^{-3} d^3 D_L N_V \Delta T / a^2 \dot{T}]}$$

where ΔT_r is the reduced undercooling and is given by $\Delta T/T_L$, d is the diameter of the droplet considered, t and $\dot{T}$ is the cooling rate before nucleation starts. If the processing parameters remain constant, it will depend only on droplet size. For small droplets, as will be discussed later, Newtonian cooling conditions can be assumed. In this case the average cooling rate can be correlated to droplet diameter following the treatment by Levi[83]

$$\dot{T} = 12(V_m/C_L)(T - T_g)K_g/d^2$$

where C_L is the heat capacity of the liquid, K_g is the heat conducitivity of the atomisation gas, T and T_g are the temperatures of the droplet and the atomisation gas, respectively. By combining Eqns (23) and (24), the relationship between T_r and droplet diameter can be established as

$$\Delta T_r^2 = \frac{16\pi\sigma_{SL}^3 V_m^2}{\left.\right]} \qquad (25)$$

The density, distribution of heterogeneous nucleants, and the volume of the droplet govern the probability of homogeneous nucleation. The problem concerning the distribution of nucleants has been discussed by several authors[84-87]. If a random distribution of nucleants is assumed, when a liquid is disintegrated into a collection of droplets, nucleants will be distributed among them. The distribution of nucleants among droplets follows the Poisson distribution. The fraction, X, of droplets that contain no nucleant is given by[86,87]

$$X = \exp(-MV_L)$$

where M is the number density of nucleant, and V_L is the volume of liquid under consideration. Regarding the catalytic potency of the nucleants, the undercooling

calculated using this equation represents an average value, because the distribution of nucleants in a single droplet is not included. In deriving this equation, the probability of forming a nucleus in a specific volume of liquid is considered to be proportional to the number of liquid atoms in connection with the surface of the nucleant. This probability is, therefore, proportional to the number of nucleants that exist in the volume of liquid. In reality, however, bulk liquid is disintegrated into fine droplets, so that the nucleants are randomly distributed into the droplets. If the number of liquid droplets is greater than the number of nucleants, some of the droplets may contain nucleants, and others may not. But in deriving Eqn (26), Wu *et al* [64] essentially assumed that each droplet of the same size containd equal number of nucleants. It is worth noting that this number may be less than one when the droplet size is small. This can be verified through multiplying the number density of the nucleant by the droplet volume.

The density of heterogeneous nucleation catalysts has been well documented by a number of authors. The results of Kelly *et al* [88], and Libera *et al* [89] show that the upper limit of the density of heterogeneous nucleation catalysts is to the order of $10^{14}m^{-3}$. The work of Turnbull[91] suggests that the nucleant density is about $10^{12}m^{-3}$. The experimental study of Kiminami[90], on the other hand, indicates that the density is only about $10^{11}m^{-3}$. The intermediate value, $10^{13}m^{-3}$, serves as an estimate. The volume of a 40 μm droplet is $3.3 \times 10^{-14}m^{-3}$. On the average, each droplet may contain 0.33 nucleant. Because it is physically impossible for a droplet to contain less than one nucleant, this average reflects the physical fact that some droplets contain one or more than one nucleant while others contains none. The undercooling calculated by Eqn (25), using the average nucleant density, underestimates the undercooling of the droplet which contains no nucleant and overestimates those of the droplets containing one or more than one nucleants. This serves to estimate the onset of nucleation during atomisation.

A comparison of the liquidus and homogeneous nucleation temperatures with the droplet temperature at the injection distance, as calculated by Wu *et al* [46], offers some insight into the possible solidification conditions of a droplet during co-injection of the ceramic particulates. Accordingly, the temperatures of liquid droplets at the injection distance are summarised in Fig. 4. As expected, the temperature of liquid droplets depends strongly on their diameter, decreasing dramatically with decreasing droplet diameter. According to the results obtained by Wu *et al* [46], at the point of injection, 230 μm droplets are still 51 K above the liquidus temperature, T_L, whereas 42 μm droplets are already 121 K below T_L. A comparison of the droplet temperatures (assuming no solidification occurred) with the homogeneous nucleation temperatures yields the following findings for droplets of different sizes during co-injection:

(a) When the droplets are greater than 98 μm, they are above the liquidus temperature, and consequently, are completly liquid, and

(b) When droplets are less than 98 μm, they fall between the liquidus and homogeneous nucleation temperatures.

However, because of the existence of heterogeneous nucleation reagents, only a small portion of such droplets may achieve the high undercooling levels required for homogeneous nucleation. Accordingly, a large population of the droplets will begin to solidify at temperatures near the liquidus temperature. Therefore, droplets in the size range smaller than 98 μm may be in three possible states at the distance of *SiC* particle injection: liquid, partially liquid, and solid. Since the difference between the calculated droplet temperature and the liquidus temperature is relatively large for small droplets, it is highly probable that small droplets may

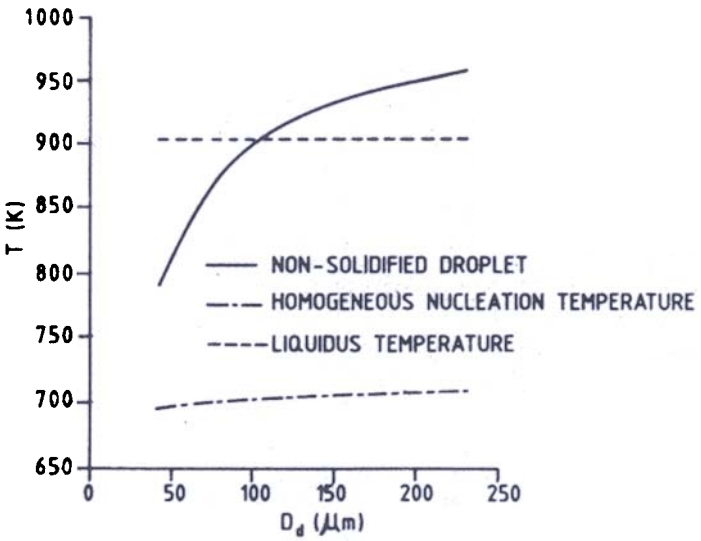

Figure 4. Calculated droplet temperatures during co-injection of ceramic particulates, and the corresponding liquidus and homogeneous nucleation temperatures, plotted as a function of the droplet diameter D_d.

experience a greater extent of pre-solidification relative to large droplets at the distance of *SiC* particle injection. This suggestion is in agreement with the experimental results which showed a decrease in *SiC* particle volume fraction with decreasing droplet size for droplets less than 98 μm in diameter. Moreover, in this size range, both surface tension and fraction solid increase with decreasing droplet size as a result of the inverse dependence of heat extraction rate on droplet size. Both of these factors will efficiently hinder the penetration of *SiC* particles during co-injection.

Moreover, the work of Wu *et al* [46] showed that the extent of incorporation of the ceramic particulates into the metallic matrix depends on the solidification condition of the droplets at the moment of *SiC* particle injection. Two factors were found to affect the distribution and volume fraction of *SiC* particles in droplets: (i) the penetration of particles into droplets; and (ii) the entrapment and/or rejection of particles by the solidification front. First, during co-injection, particles collide with the atomised droplets with three possible results: they may penetrate the droplets, adhere to the droplet surface or bounce back after impact. The extent of penetration of *SiC* particles into droplets was noted to depend on the kinetic energy of the particles, and the magnitude of the surface energy change in the droplets that occurs upon impact. In liquid droplets, the extent of penetration of *SiC* particles was shown to depend on the changes in surface energy, E_s, experienced by the droplets. Accordingly, large *SiC* particles encountered more resistance to penetration relative to small ones. In solid droplets, the penetration of *SiC* particles was correlated with the dynamic pressure exerted by the *SiC* particles on the droplets during impact, and the depth of the ensuing crater. The results showed that no penetration was possible in such droplets. Once *SiC* particles have penetrated droplets, their final location in the microstructure is governed by their interactions with the solidification front. As a result of these interactions, both entrapment and rejection of *SiC* particles occurred during droplet solidification. A comparison of the experimental results to those anticipated from well established kinetic and thermodynamic models led to some interesitng findings. First, the models proposed by Bolling and Chernov predict relative low critical interface velocities necessary for entrapment, inconsistent with the experimental findings reported by Wu *et al* [46]. Although the reported correlation between the critical front velocity and droplet diameter was generally consistent with that predicted by Stefanescu's model[51], the dependence on the size of *SiC* particles was not. In view of this discrepancy, three possible mechanisms were proposed to account for the experimental findings: nucleation of *a–Al* on *SiC* particles; entrapment of *SiC* particles in between primary dendrite arms; and entrapment of *SiC* particles in between secondary dendrite arms. Further work is in progress in this area.

7. STATUS OF SPRAY AUTOMISATION AND DEPOSITION RESEARCH IN INDIA

Presently, research activities involving spray atomisation and co-deposition processing are at a nascent stage in India. Prof Ojha (Department of Metallurgy, Institute of Technology, Varanasi), has developed a small experimental spray deposition apparatus, capable of handling approximately half a kilogram of melt. Also Prof Ranganathan (Indian Institute of Science (IISC), Bangalore), along with Prof Ojha is pursuing research on various spray deposited materials, including *Al–Si* and *Al–Pb* alloys.

More recently, the National Physical Laboratory (NPL), New Delhi and the IISC, Bangalore, have jointly submitted an Indo-US collaborative project entitled: 'Processing, microstructural characterisation and properties of aluminium-based metal-matrix composites processed using spray atomisation and co-deposition technique'. The proposal envisages setting up a spray deposition facility at NPL, and subsequently developing MMCs and other materials using this technique. NPL, New Delhi has excellent processing facilities and is currently engaged in studying hot deformation behaviour of various advance structural materials.

8. CONCLUSION

The development of spray atomisation and deposition processes for the manufacture of particulate reinforced MMCs was motivated by the difficulties associated with the currently available casting and powder metllurgical processes. In principle, such an approach will inherently avoid the extreme thermal excursions, with concomitant degradation in interfacial properties and extensive macrosegregation, normally associated with casting processes. Furthermore, this

approach also eliminates the need to handle fine reactive particulates, as is necessary with powder metallurgical processes. The results discussed in the present work demonstrate that the preliminary findings obtained with this synthesis approach are encouraging. It is also evident, however, that it will be necessary to develop ar. in-depth understanding of the fundamental physical phenomena invloved, before such a process can measure up to its commercial potential. The latter will be a challenging task for the scientific community, in view of the complex fluid, thermal and solidification phenomena invloved.

ACKNOWLEDGEMENTS

The author is grateful to the Army Research Office financial support and encouragement and Dr P Rama Rao (Dept of Science and Technology, India) for his kind invitation to contribute this paper.

REFERENCES

Knight, R.; Smith, R.W. & Apelian, D. Application of plasma arc melting technology to processing of reactive metals. *Int. Mater. Rev.*, 1991, **36**, 221-52.

2. Mendiratta, M.G.; Ehlers, S.K.; Chatterje, D.K. & Lipsitt, H.A. Tensile flow and fracture behaviour of DO_3Fe-25 at. pct *Al* and *Fe*-31 at pct alloys. *Metall. Trans.*, 1987, **18A**, 283-91.
3. Horton, J.A.; Liu, C.T. & Koch, C.C. *In* High temperature alloys: theory and design, Edited by J.O. Stiegler, The Metallurgical Society. Warrendale, 1984. pp. 309.
4. Das, S.K. & Davis, L.A. High performance aerospace alloys via rapid solidification processing. *Mater. Sci. Eng.*, 1988, **A98**, 1-12.
5. Lavernia, E.J.; Ayers, J.D. & Srivatsan, T.S. Rapid solidification processing with specific application to aluminium alloys. *Int. Mater. Rev.*, 1992, **1**(37), 1-44
6. Singer, A.R.E. Aluminium and aluminium-alloy strip produced by spray deposition and rolling. *J. Inst. Met.*, 1972, **100**, 185-90.
7. Lavernia, E.J. The evolution of microstructure during spray atomisation and deposition. *Int. J. Rap. Soli.*, 1989, **5**, 47-85.
8. Liang, X. & Lavernia, E.J. Solidification and microstructure evolution during spray atomisation and deposition of Ni_3Al. *Mater. Sci. Eng.*, 1993, **A161**, 221-35.
9. Liang, X. & Lavernia, E.J. Microstructure evolution during the spray deposition of Ni_3Al and Ni_3Al composites. *JOM*, 1993, **45**(7), 50-55.
10. Mathur, P.; Annavarapu, S.; Apelian, D. & Lawley, A. Process control, modeling and applications off spray casting. *J. Met.*, 1989, **41**(10), 23-28.
11. Doherty, R.D. First international conference on spray forming swansea, UK, September 1990. *Int. J. Pow. Metall.*, 1991, **27**(1), 67-69.
12. Lavernia, E.J.; Rai, G. & Grant, N.J. Rapid solidification processing of 7XXX aluminium alloy: a review. *Mater. Sci. Eng.*, 1985, **79**(2), 211-21.
13. Savage, S.J. & Froes, F.H. Production of rapidly solidified metals and alloys. *JOM*, 1984, **36**(4), 20-33.
14. Lavernia, E.J.; Baram, J. & Gutierrez, E. Precipitation and excess solid solubility in *Mg-Al-Zr* and *Mg-Zn-Zr* processed by spray atomisation and deposition. *Mater. Sci. Eng.*, 1991, **A132**, 119-33.
15. Lavernia, E.J.; Gomez, E. & Grant, N.J. The structures and properties of *Mg-Al-Zr* and *Mg-Zn-Zr* alloys produced by LDC. *Mater. Sci. Eng.*, 1987, **A95**, 225-36.
16. Marinkovich, J.M.; Mohamed, F.A.; Pickens, J.R. & Lavernia, E.J. The spray atomisation and deposition of Weldalite 049. *JMO*, 1989, **41**(9), 36-41.
17. Estrada, J.L. & Duszczyk, J. Characteristics of rapidly solidified *Al-Si-X* preforms produced by the osprey process. *J. Mater. Sci.*, 1990, **25**(2B), 1381-91.
18. Ojha, S.N.; Jha, J.N. & Singh, S.N. Microstructural modifications in *Al-Si* eutectic alloy produced by spray deposition. *Scr. Metall. et Mater.*, 1991, **25**(2), 443-47.
19. Desanctis, M. Structure and properties of rapidly solidified ultrahigh strength *Al-Zn-Mg-Cu* alloys produced by spray deposition. *Mater. Sci. Eng.*, 1991, **A141**, 103-21.
20. Machler, R.; Uggowitzer, P.J.; Solenthaler, C. & Pedrazzoli, R.M. Structure, mechanical

properties, and stress corrosion behaviour of high strength spray deposited 7000 series aluminium alloy. *Mater. Sci. & Tech.*, 1991, **7**, 447-51.

21 Baram, J. Structure and properties of a rapidly solidified *Al-Li-Mn-Zr* alloy for high-temperature applications 2. Spray atomisation and deposition processing. *Metall. Trans. A*, 1991, **22**, 2515-22.

22 Zhou, J.; Duszczyk, J. Effect of extrusion conditions on mechanical properties of *Al-20Si-3Cu-1Mg* alloy prepared from rapidly solidified power. *J. Mater. Sci.*, 1991, **26**(19), 3739-47.

23 Ebalard, S. & Cohen, M. Structural and mechanical properties of spray cast-iron. *Mater. Sci. Eng.*, 1991, **A133**, 297-300.

24 Annavarapu, S.; Apelian, D. & Lawley, A. Processing effects in spray casting of steel strip. *Metall. Trans. A*, 1988, **19A**, 3077-86.

25 Igharo, M. & Wood, J.V. Investigation of M2 high speed steel produced by Osprey process. *Pow. Metall.*, 1989, **32**(2), 124-31.

26 Ikawa, Y.; Itami, T.; Kumagai, K. & Kawashima, Y. Spray deposition method and its application to the production of mill rolls. *ISIJ Int.*, 1990, **30**(9), 756-63.

27 Annavarapu, S.; Apelian, D. & Lawley, A. Spray casting of steel strip—process analysis. *Metall. Trans. A*, 1990, **22**, 3237-56.

28 Ucok, I.; Ando, T. & Grant, N.J. Property enhancement in type 316L stainless steel by spray forming. *Mater. Sci. Eng.*, 1991, **A133**, 284.

29 Ojha, S.N. & Singh, S.N. On spray deposition of high-speed steel. *J. Mater. Sci. Let.*, 1991, **10**(15), 893-95.

30 Mathur, P.; Annavarapu, S.; Apelian, D. & Lawley, A. Spray casting - an integral model for process understanding and control. *Mater. Sci. Eng.*, 1991, **142**(2), 261-76.

31 Singh, R.P.; Lawley, A. Friedman, S. & Murty, Y.V. Microstructure and properties of spray cast *Cu-Zr* alloys. *Mater. Sci. & Engg.*, 1991, **145**(2), 243-55.

32 Bricknell, R.H. The structure and properties of a nickel-base superalloys produced by Osprey atomisation and deposition. *Metall. Trans. A*, 1986, **17A**, 583-91.

33 Moran, A.L. & White, D.R. Developing intelligent control for spray forming processes. *JOM*, 1990, **42**(7), 21-24.

34 Harada, T.; Ando, T.; Ohandley, R.C. & Grant, N.J. A microstructural study of a $Nd_{15}Fe_{77}B_8$ magnetic alloy produced by liquid dynamic compaction (LDC). *Mater. Sci. Eng.*, 1991, **A133**, 780-84.

35 Harada, T.; Ando, T.; Ohandley, R.C. & Grant, N.J. Structures and magnetic properties of a $Nd_{15}Fe_{77}B_8$ alloy produced by twin-roller quenching. *J. App. Phys.*, 1990, **68**, 4728-33.

36 Bewlay, B.P. & Cantor, B. The relationship between thermal history and microstructure in spray-deposited tin-lead alloys. *J. Mater. Res.*, 1991, **6**(7), 1433-54.

37 Vetter, R.; Zhuang, L.Z.; Majewska-Glabus, I. & Duszczyk, J. Microstructure of the Osprey processed *Cr*-containing Ni_3Al-*X* intermetallic in conjunction with solidification model at the deposition. *Scr. Metall. et Mater.*, 1990, **24**, 2025-30.

38 Zhuang, L.Z.; Majewska-Glabus, I.; Vetter, R. & Duszczyk, J. A modified spray deposition model verified with Ni_3Al-*Cr* intermetallic alloys. *Scr. Metall. et Mater.*, 1990, **24**, 2089-94.

39 Liang, X.; Earthman, J.C. & Lavernia, E.J. On the mechanism of grain formation during spray atomisation and deposition. *Acta Met. et Mat.*, 1992, **40**, 3003-16.

40 Morris, D.G. & Morris, M.A. Rapid solidification of Ni_3Al by Osprey deposition. *J. Mater. Res,.* 1991, **6**, 361-65.

41 Sears, J.W. Titanium spray formed structures in advances in power metallurgy & particulate Materials 1992, Vol. 1, MPIF, Princeton, New Jersey.

42 White, J.; Palmer, I.G.; Hughes, I.R. & Court, S.A. *In.* Aluminium-lithium alloys, Vol 3, edited by T.H. Sanders, Jr. & E.A. Starke, Jr. MCE, Williamsburg, 1989. pp. 1635.

43 Gupta, M. Mohamed, F.A. & Lavernia, E.J. The effects of solidification phenomena on the distribution of *SiC* particulates during spray atomisation and co-deposition. *Int. J. Rap. Soli.*, 1991, **6**, 247-84.

44. Singer, A.R.E. Metal matrix composities made by spray forming. *Mater. Sci. Eng.*, 1991, **A35**, 13-17.

45. Gupta, M.; Mohamed, A. & Lavernia, E.J. Heat transfer mechanisms and their effects on microstructure during spray atomisation and codeposition of matrix composites. *Mate·. Sci. Eng.*, 1991, **A144**, 99-110.

46. Wu, Y. & Lavernia, E.J. Interaction mechanisms between ceramic particles and atomised metallic droplets. *Met. Trans. A*, 1992, **23A**, 2923-37.

47. Gupta, M.; Mohamed, F.A. & Lavernia, E.J. The effect of ceramic rei.forcements during spray atomisation and codeposition of metal matrix composites. I. Heat transfer. *Met. Trans. A*, 1992, **23**, 831-43.

48. Gupta, M.; Mohamed, F.A. & Lavernia, E.J. The effect of ceramic reinforcements during spray atomisation and codeposition of metal matrix composites. II. Solid-state cooling effects. *Met. Trans. A*, 1992, **23A**, 845-50.

49. Zeng, X.L.; Liu, H.M.; Chu, M.G. & Lavernia, E.J. An experimental investigation of reactive atomisation and deposition processing of Ni_3Al/Y_2O_3 using N_2-O_2 atomisation. *Met. Trans. A*, 1992, **23A**, 3394-99.

50. Rohatgi, P.K.; Asthana, R.; Yadav, R.N. & Ray, S. Energetics of particle tranfer from gas to liquid during solidification processing of composites. *Met. Trans. A*, 1990, **21A**, 2073-82.

51. Stefanescu, D.M.; Dhindaw, B.K.; Kacar, S.A. & Moitra, A. Behaviour of ceramic particles at the solid-liquid metal interface in metal matrix composites. *Met. Trans. A*, 1988, **19A**, 2847-55.

52. Rohatgi, P.K.; Asthana, R. & Das, S. Solidification, structures, and properties of cast metal-ceramic particle composites. *Int. Mat. Rev.*, 1988, **31**, 115-39.

53. Kanetkar, C.S.; Kacar, A.S. & Stefanescu, D.M. The wetting characteristics and surface tension of some *Ni*-based alloys on yttria, hafnia, alumina, and zirconia substrate. *Met. Trans. A*, 1988, **19A**, 1833-39.

54. Stefanescu, D.M.; Moitra, A.; Kacar, A.S. & Dhindaw, B.K. The influence of buoyant forces and volume fraction of particles on the particle pushing/entrapment tranisition during directional solidification of *Al/SiC* and *Al*/Graphite composites. *Met. Trans. A*, 1990, **21A**, 231-39.

55. Nath, D.; Narayan, R. & J. Rohatgi, P.K. Damping capacity, resistivity, thermal expansion and machinability of aluminium alloy-mica composites. *J. Mater. Sci.*, 1981, **16**, 3025-32.

56. Kacar, A.S.; Rana, F. & Stefanescu, D.M. Kinetics of gas-to-liquid transfer of particles in metal matrix composites. *Mater. Sci. Eng.*, 1991, **A135**, 95-100.

57. Kojima, K.A.; Lewis, R.E. & Kaufman, M.J. *In* Aluminium-Lithium alloys Vol. 1, edited by Sanders, T.H. Jr. & Starke, E.A. Jr MCE, Williamsburg, MCE, 1989. p. 85.

58. Ibrahim, I.A.; Mohamed, F.A. & Lavernia, E.J. Particulate reinforced metal matrix composites - a review. *J. Mater. Sci.*, 1991, **25**, 1137-56.

59. Chanda, T.; Lavernia, E.J. & Wolfenstine, J. Hot deformation of particulate reinforced *Al-4Li-1Mg-0.5Ge-0.2Zr*. *Scr. Met. et Mat.*, 1991, **25**, 131-35.

60. Willnecker, R.; Herlach, D.M. & Feuerbacher, B. Grain refinement induced by a critical crystal growth vrlocity in undercooled melts. *Applied Physics Letters*, 1990, **56**, 324-26.

61 Rack, H.J. & Holloway, P.H. Grain boundry precipitation in 18*Ni* maraging steels. *Met. Trans. A*, 1977, **8A**, 1313-15.

62. Ratnaparkhi, P.L. & Rack, H.J. Aging effects on the fracture toughness of *SiC*-whisker-reinforced 2XXX aluminium alloys. *Scr. Metall. et Mater.*, 1989, **23**, 2143-46.

63. Rack, H.J. Metal-matrix composites. *Adv. Mater. Proc.*, 1990, **137**, 37-38.

64. Ratnaparkhi, P.L. & Rack, H.J. Crack growth in oriented *SiC*-whisker-reinforced 2124 aluminium composites. *Mat. Sci. Eng.*, 1990, **A129**, 11-19.

65. Vogelsang,; M. Arsenault, R.J. & Fisher, R.M. An in-situ HVEM study of dislocation generation at *Al/SiC* interfaces in metal matrix composites. *Met. Trans.*, 1986, **17A**, 379-89.

66. Zhang, J.; Perez, R.J. & Lavernia, E.J. Dislocation-induced damping in metal matrix composites. *J. Mater. Sci.*, 1993, **28**, 835-46.

67. Chu, M.G.; Denzer, D.K.; Chakrabarti, A.K. & Billman, F. Evalution of aluminium and nickel alloy materials produced by spray deposition. *Mat. Sci. Eng.*, 1988, **A98**, 227- 32.

68. Gupta, M.; Juarez-Islas, J.; Frazier, W.E.; Mohamed, F.A. & Lavernia, E.J. Microstructure, excess solid solubility, and elevated-temperature mechanical behaviour of spray-atomised and codeposited *Al-Ti-SiC$_p$*. *Met. Trans. B*, 1992, **23A**, 719- 36.

69. Mirchandani, P.K. & Benn, R.C. Experimental high modulus elevated temperature *Al-Ti* based alloys by mechanical alloying, 1988, SAMPE, Covina, CA.

70. Frazier, W.E. & Koczak, M.J. Elevated temperature aluminium-titanium alloy by powder metallurgy process, US patent, No. 4,834,942, 1989.

71 Frazier, W.E.; Lee, E.W.; Donnellan, W.E. & Thompson, J.J. Advanced lightweight alloys for aerospace applications. *JOM*, 1989, **41**(5), 22-26.

72 Fine, M.E. Stablity and coarsening of dispersoids in aluminium alloys. *In* Dispersion strengthened aluminium alloys, edited by Kim, Y.W. and Griffith, W.M. TMS, Warrendale, 1988. p. 103.

73 Gupta, M.; Mohamed, F.A. & Lavernia, E.J. Solidification characteristics of atomised *Al-Ti* powders *Scrip. Met. et Mat.*, 1992, **26**, 697-702.

74 Gutierrez-Miravete, E.; Trapaga, G. & Szekely, J. *In* Casting of near net shape products, edited by Y. Sahai, J.E. Battles, R.S. Carbonara, & Mobley, C.E. The Metallurgical Society, 1988. p. 133.

75 Mathur, P.; Apelian, D. & Lawley, A. Analysis of the spray deposition process. *Acta Metall.*, 1989, **37**, 429-43.

76. Lavernia, E.J.; Gutierrez, E.; Szekely, J. & Grant, N.J. A mathematical model of the LDC process. Part 1: heat flow in gas atomisation. *Int. J. of R.S.*, 1988, **4**, 89-124.

77. Gutierrez, E.; Lavernia, E.J. Trapaga, G. & Szekely, J. A mathematical model of the LDC process. Part 1: heat flow in gas atomisation. *Int. J. of R.S.*, 1988, **4**, 125-50.

78. Gutierrez, E.; Lavernia, E.J.; Trapaga, G.; Szekely, J. & Grant, N.J. A mathematical model of the spray deposition process. *Metall. Trans.*, 1989, **20A**, 71-85.

79. Liang, X. & Lavernia, E.J. Interfacial behaviour in a *Ni_3Al/TiB_2* intermatallic matrix composite. *Mat. Sci. Eng.* , 1992, **A153**, 654-61.

80. Liang, X.; Earthman, J.C. & Lavernia, E.J. Microstructure and elevated temperature behaviour of a spray-atomised and co-deposited *$Ni_3Al/SiC/TiB_2$* intermetallic matrix composite. *Mat. Sci. Eng.*, 1992, **A153**, 646-53.

81 Hirth, J.P. Nucleation, undercooling and homogeneous structures in rapidly solidified powders. *Metall. Trans. A.*, 1978, **9A**, 401-04.

82. Thompson, C.V. & Spaepen, F. Homogeneous crystal nucleation in binary melts. *Acta Metall.*, 1983, **31**, 2021-27.

83 Levi, C.G. & Mehrabian, R. Heat flow during rapid solidification of undercooled metal droplets. *Metall. Trans.*, 1982, **13A**, 221-34.

84 Chen, I.W., Chiao, Y.H. & Tsuzaki, K. Statistics of martensitic nucleation. *Acta Metall.*, 1985, **33**, 1847-59.

85. Perepezko, J.H. & Paik, J.S. *In* Rapidly solidified amorphous and crystalline alloys, edited by B.H. Kear, B.C. Giessne. M. Cohen, North Holland, Amsterdam, 1982. p. 49.

86. Perepezko, J.H. Nucleation in undercooled liquids. *Mater. Sci. Eng.*, 1984, **A65**, 125-35.

87. Drehman, A.J. & Tunbull, D. Solidification behaviour of undercooled *$Pd_{83}Si_{17}$* and *Pd_{82} Si_{18}* liquid droplets. *Scri. Metall.*, 1981, **15**, 543-48.

88. Kelley, T.F.; Cohen, M. & Vander Sande, J.B. Rapid solidification of a droplet - processed stainless steel. *Metall. Trans.* 1984, **15A**, 819-33.

89. Libera, M.R. & Vander Sande, J.B. Heterogeneous nucleation of solidification in atomised liquid metal droplets. *Mater. Sci. Eng.*, 1991, **A132**, 107-18.

90. Kiminami, C.S. Influence of heterogeneous nuclei on the solidification of *$Pd_{77.5}Cu_6Si_{16.5}$* glassy alloy. *Mater. Sci. Eng.*, 1988, **A97**, 195-98.

91 Turnbull, D. Under what conditions can a glass be formed? *Contemp. Phys.*, 1969, **10**, 473-88.